Magnetic properties of polydisperse ferrofluids: A critical comparison between experiment, theory, and computer simulation

Alexey O. Ivanov
Department of Mathematical Physics, Urals State University, 51 Lenin Avenue, Ekaterinburg 620083, Russia

Sofia S. Kantorovich and Evgeniy N. Reznikov
Department of Mathematical Physics, Urals State University, 51 Lenin Avenue, Ekaterinburg 620083, Russia;
Frankfurt Institute for Advanced Studies, Johann Wolfgang Goethe Universität,
Max-von-Laue Strasse 1, D-60438 Frankfurt am Main, Germany;
and Max-Planck-Institut für Polymerforschung, Ackermannweg 10, D-55128, Mainz, Germany

Christian Holm
Frankfurt Institute for Advanced Studies, Johann Wolfgang Goethe Universität,
Max-von-Laue Strasse 1, D-60438 Frankfurt am Main, Germany
and Max-Planck-Institut für Polymerforschung, Ackermannweg 10, D-55128, Mainz, Germany

Alexander F. Pshenichnikov and Alexander V. Lebedev
Institute of Continuous Media Mechanics, 1 Korolyev Street, 614013 Perm, Russia

Alexandros Chremos and Philip J. Camp*
School of Chemistry, University of Edinburgh, West Mains Road, Edinburgh EH9 3JJ, United Kingdom
(Received 30 December 2006; published 28 June 2007)

Experimental magnetization curves for a polydisperse ferrofluid at various concentrations are examined using analytical theories and computer simulations with the aim of establishing a robust method for obtaining the magnetic-core diameter distribution function $p(x)$. Theoretical expressions are fitted to the experimental data to yield the parameters of $p(x)$. It is shown that the majority of available theories yield results that depend strongly on the ferrofluid concentration, even though the magnetic composition should be fixed. The sole exception is the second-order modified mean-field (MMF2) theory of Ivanov and Kuznetsova [Phys. Rev. E **64**, 041405 (2001)] which yields consistent results over the full experimental range of ferrofluid concentration. To check for consistency, extensive molecular dynamics and Monte Carlo simulations are performed on systems with discretized versions of $p(x)$ corresponding as closely as possible to that of the real ferrofluid. Essentially perfect agreement between experiment, theory, and computer simulation is demonstrated. In addition, the MMF2 theory provides excellent predictions for the initial susceptibility measured in simulations.

DOI: 10.1103/PhysRevE.75.061405 PACS number(s): 82.70.Dd, 75.50.Mm, 82.20.Wt

I. INTRODUCTION

Ferrofluids are colloidal suspensions of single-domain, homogeneously magnetized particles with diameters in the region of 10 nm [1]. One of the defining characteristics of ferrofluids is the tendency of the constituent particles to self-assemble into a variety of cluster types, including chains, rings [2–5], and other more exotic shapes [6], when the dipole-dipole interaction energy between particles is sufficiently large as compared to the thermal energy. The topologies of the clusters are largely dictated by the energetically favorable "nose-to-tail" conformation of two dipoles. The formation of chainlike clusters is strongly enhanced by applied magnetic fields and can profoundly affect the observed rheological and optical properties of the fluid. As a result of this sensitivity, ferrofluids are employed in a wide range of applications as "switchable" fluids. It is therefore very important to characterize the response of a magnetic fluid to an applied magnetic field. This is most commonly achieved by measuring the magnetization curve $M(H)$, that is, the dependence of the scalar magnetization $M=|\boldsymbol{M}|$ on the magnetic field strength $H=|\boldsymbol{H}|$; both quantities have dimensions of A m^{-1}. In addition, the initial susceptibility $\chi=dM/dH|_{H=0}$ is an important parameter for determining the response of the magnetization to small fields (within the linear-response regime).

The most widely studied ferrofluids are based on colloidal magnetite (Fe_3O_4). Each colloidal particle contains a homogeneously magnetized core with diameter x, plus a nonmagnetic surface coating of thickness $l\sim 2$ nm to effect steric stabilization against irreversible aggregation. Due to demagnetization and chemical sorption effects at the boundary of the magnetic core, there is also a layer of demagnetized magnetite of thickness $\delta\sim 1$ nm. In most cases the particles show strong size polydispersity, with a magnetic-core diameter probability distribution function $p(x)$. The nonmagnetic colloidal interactions are sensitive to the nature of the surface layers and the carrier solvent. In the ferrofluids considered here, the organic coating and carrier solvent can be consid-

*Corresponding author. Electronic address: philip.camp@ed.ac.uk

ered index matched, so that the effective nonmagnetic interaction is short-ranged and repulsive. As a consequence, in the overwhelming majority of theoretical studies, such ferrofluids are modeled quite faithfully as dipolar hard spheres with an effective particle diameter $\sigma \simeq x+\sigma_0$, where $\sigma_0=2\delta+2l$. The particle dipole moment is given by

$$\mu(x) = \frac{\pi}{6} M_s x^3, \tag{1}$$

where M_s is the bulk saturation magnetization of the core material: for magnetite at $T=293$ K, $M_s=4.8\times10^5$ A m^{-1}. Experimental data obtained by Pshenichnikov and coworkers are considered in this work [7,8]. Results for a magnetite colloid dispersed in kerosene were obtained at seven concentrations corresponding to fluid saturation magnetizations in the range $5.0 \leqslant M_\infty \leqslant 57.0$ kA m^{-1}. The fluid saturation magnetization is defined by

$$M_\infty = \lim_{H\to\infty} M(H) = \frac{\pi\rho M_s}{6}\langle x^3\rangle, \tag{2}$$

where $\rho=N/V$ is the number of particles (N) per unit volume (V), and the angled brackets denote an average over the magnetic-core diameter probability distribution function $p(x)$: $\langle f(x)\rangle=\int_0^\infty p(x)f(x)dx$. Crucially, the samples at the seven concentrations were obtained by dilution of a stock concentrated ferrofluid, and hence the magnetic composition [encoded by $p(x)$] should be identical for each sample. The experimental data in Ref. [8] show very little random scatter, and are clearly suitable for testing the predictions of theory and simulation. For the experimental details of this earlier work, consult Refs. [7,8].

Theoretical and simulation approaches to $M(H)$ and χ are frustrated by incomplete knowledge of the nanoparticle polydispersity—as characterized by $p(x)$—and the precise nature of the nonmagnetic interactions mediated by the nonmagnetic coating and carrier solvent. From a theoretical standpoint, the moments of $p(x)$ have to be determined from an analysis of experimental measurements of $M(H)$ and χ assuming that the theory can be relied upon to predict with sufficient accuracy the magnetic properties of a fluid with prescribed $p(x)$ and short-range (nonmagnetic) interactions. The formidable problems associated with describing fluids of strongly interacting particles are well known [9–11], and strongly correlated dipolar systems are particularly difficult to handle due to the anisotropy and long range of the interactions, and some subtle effects of boundary conditions [12]. The challenge is therefore to identify an analytical theory capable of describing the properties of ferrofluids over wide ranges of temperature and concentration. There have been many candidate theories put forward over the last century, including Langevin's single-particle model [13], Weiss's mean-field model [14,15], the "mean-spherical approximation" (MSA) closure of the Ornstein-Zernike equation [16,17], a high-temperature approximation (HTA) [18,19], first-order [8] and second-order modified mean-field models [20,21], and a Born-Mayer cluster-expansion (CE) theory [22,23]. One of the goals of this work is to effect a critical comparison of the aforementioned theories in terms of the apparent moments $\langle x^n\rangle$, determined by analyzing experimental magnetization curves. If a theory is capable of describing the properties of a magnetic fluid with fixed magnetic composition over a wide range of concentration, then the values of those moments should be independent of concentration. The first main result of this paper is that only the second-order modified mean-field (MMF2) theory satisfies this criterion. It will also be shown that the MMF2 theory appears to be the most accurate theory yet formulated for the magnetic properties of ferrocolloid suspensions.

In principle, Monte Carlo (MC) and molecular dynamics (MD) computer simulations yield essentially exact results for the microscopic structure and bulk-phase properties of materials [24]. The utility of such techniques in determining the particle polydispersity in real ferrofluids is, however, limited because of the difficulty of conducting real-time optimization of the system parameters by comparison with experimental results. Nevertheless, because the representation of interparticle correlations is essentially exact, computer simulations can be used to validate specific choices of the magnetic-core diameter distribution by comparison with experiment. Moreover, for a given molecular model and magnetic-core diameter distribution, computer simulations provide critical tests of specific approximations required to derive a tractable analytical theory.

In this paper, a critical comparison is made between magnetization curves for a polydisperse ferrofluid obtained by experiment, theory, and simulation. The results confirm that the MMF2 theory provides a completely consistent description of $M(H)$ over the full range of ferrofluid concentrations studied in experiments and simulations. In addition, simulation measurements of the initial susceptibility χ are shown to be in excellent agreement with the predictions of MMF2 theory, thus providing yet further support for that theoretical approach. On a technical note, it is also shown that great care must be taken when simulating polydisperse ferrofluids, particularly with regard to the method of discretizing the magnetic-core diameter distribution. The paper is organized as follows. Section II contains a specification of the polydisperse dipolar sphere model, and a summary of the theoretical and simulation methods employed in this work. The results are presented in Sec. III, and Sec. IV concludes the paper.

II. MODEL AND METHODS

A. Polydisperse dipolar spheres

The experimental studies of Pshenichnikov *et al.* [8] show that a suitable description of the magnetic-core diameter polydispersity is provided by the Γ distribution [25]

$$p(x) = \frac{x^\alpha \exp(-x/x_0)}{x_0^{\alpha+1}\Gamma(\alpha+1)}, \tag{3}$$

where αx_0 is the most probable value of x. The nth moment of $p(x)$ is given by

$$\langle x^n \rangle = x_0^n \prod_{k=1}^{n} (\alpha + k). \tag{4}$$

The Γ distribution is preferred because it has a rapidly decaying, exponential tail at large x, and the higher moments are smaller than those of other candidate distributions such as the log-normal distribution. This is important because $M_\infty \propto \langle x^3 \rangle$, and $\chi \propto \langle x^6 \rangle$, and so the key experimental parameters of ferrofluids are sensitive to such high moments [8]. Obviously, one of the key tasks is to identify the parameters x_0 and α on the basis of experimental data. The determination of these parameters by comparison of experiment and analytical theory is described in Sec. III A.

In theory and in simulations, the ferrofluid is modeled by a polydisperse dipolar sphere system, defined by the pair-interaction potential

$$u(\boldsymbol{r}_{ij}, \boldsymbol{\mu}_i, \boldsymbol{\mu}_j) = u^{SR}(r_{ij}) + \frac{\mu_0}{4\pi}\left(\frac{(\boldsymbol{\mu}_i \cdot \boldsymbol{\mu}_j)}{r_{ij}^3} - \frac{3(\boldsymbol{\mu}_i \cdot \boldsymbol{r}_{ij})(\boldsymbol{\mu}_j \cdot \boldsymbol{r}_{ij})}{r_{ij}^5} \right), \tag{5}$$

where $u^{SR}(r_{ij})$ is the isotropic nonmagnetic interaction potential, $\boldsymbol{r}_{ij}$ is the center-center separation vector, $r_{ij} = |\boldsymbol{r}_{ij}|$, $\mu_0 = 4\pi \times 10^{-7}$ H m^{-1} is the vacuum magnetic permeability, and $\boldsymbol{\mu}_i$ is the dipole moment on particle i. The specific choice of short-range interaction (soft sphere or hard sphere) depends on theoretical and simulation convenience. Unless there is strong aggregation (in which case short-range interactions will be important) any resulting variations in fluid structure and magnetic properties are likely to be negligible [20]. The specific details of $u^{SR}(r_{ij})$ are given in Secs. II D and II E. The interaction energy between dipole i and the applied field is $-\mu_0 \boldsymbol{\mu}_i \cdot \boldsymbol{H}$.

B. Summary of theoretical models

In this section, brief summaries of various theoretical approaches to $M(H)$ are given in roughly chronological order. It is not intended to provide comprehensive details of each approach, rather it summarizes the key equations, and gives some brief indications of their origins. The reader is referred to the original literature for further details.

Langevin model. The simplest ferrocolloid model ignores interparticle interactions, and hence the statistical-mechanical problem reduces to the calculation of single-particle partition functions; this is Langevin's one-particle model [13]. The calculations are elementary, and for a polydisperse collection of noninteracting dipolar particles, the resulting magnetization curve is given by

$$M_L(H) = \rho \left\langle \mu(x) L\left(\frac{\mu_0 \mu(x) H}{k_B T} \right) \right\rangle, \tag{6}$$

where the "Langevin" function is defined by

$$L(z) = \coth z - \frac{1}{z}. \tag{7}$$

The Langevin initial susceptibility χ_L is

$$\chi_L = \frac{\mu_0 \rho \langle \mu^2(x) \rangle}{3 k_B T}. \tag{8}$$

Weiss model. Interactions can be taken in to account at a mean-field level by considering how the fluid magnetization augments the applied magnetic field [14,15]. The additional contribution is proportional to the fluid magnetization, and assuming a prefactor equal to the Lorentz value, the effective field is

$$H_e = H + \frac{1}{3} M(H). \tag{9}$$

The resulting magnetization curve (Weiss' model) is then given by

$$M(H) = \rho \left\langle \mu(x) L\left(\frac{\mu_0 \mu(x) H_e}{k_B T} \right) \right\rangle. \tag{10}$$

This expression is a transcendental equation for $M(H)$, and hence $M(H)$ depends on the number density ρ in a nonlinear way. The Weiss expression for the initial susceptibility χ in terms of the Langevin susceptibility χ_L has the form

$$\chi = \frac{\chi_L}{1 - (1/3)\chi_L}. \tag{11}$$

Mean-spherical approximation. The mean spherical approximation (MSA) provides a closure to the Ornstein-Zernike equation [12] which, in the case of dipolar hard spheres, leads to closed-form expressions for thermodynamic properties [16]. This has been extended to magnetic fluids in arbitrary applied magnetic fields by Morozov and Lebedev [17]. The magnetization curve is expressed with the nonlinear equation

$$M(H) = \rho \left\langle \mu(x) L\left(\frac{\xi \mu_0 \mu(x) H}{k_B T} \right) \right\rangle, \tag{12}$$

where ξ is given by

$$\xi = \frac{1}{q(AF)}\left(1 + \frac{M(H)(1+A)}{3H} \right) = \frac{1}{q(BF)}\left(1 + \frac{M(H)(1+B)}{3H} \right). \tag{13}$$

The parameters A and B are the roots of the equation $35z^2 - 5(10-3\beta)z - 7(7+3\beta) = 0$ where $\beta = d \ln M(H) / d \ln(\xi H)$. The parameter F satisfies the equation

$$\chi_L = \chi q(-F) = q(2F) - q(-F), \tag{14}$$

where $q(z) = (1+2z)^2/(1-z)^4$. Equation (14) defines the MSA susceptibility, $\chi = \chi_L / q(-F)$.

High-temperature approximation. A systematic perturbation expansion in terms of a dipolar coupling parameter (proportional to $\mu_0 \mu^2 / 4\pi k_B T$) truncated at first order yields the high-temperature approximation (HTA) [18,19]. The result is that the effect field H_e is given in terms of the derivative of the Langevin magnetization $M_L(H)$:

$$M(H) = M_L(H)\left(1 + \frac{1}{3}\frac{dM_L(H)}{dH}\right). \tag{15}$$

Similarly, the HTA expression for the initial susceptibility is couched in terms of the Langevin initial susceptibility:

$$\chi = \chi_L\left(1 + \frac{1}{3}\chi_L\right). \tag{16}$$

First-order modified mean-field model. Pshenichnikov and co-workers put forward a natural variation on Weiss's mean-field model to yield the first-order modified mean-field (MMF1) theory. The basic idea is to replace $M(H)$ in Eq. (9) with the Langevin magnetization (6) which is linearly dependent on concentration. The resulting expressions (which are no longer transcendental) are

$$M(H) = \rho\left\langle \mu(x)L\left(\frac{\mu_0\mu(x)H_e}{k_BT}\right)\right\rangle, \tag{17}$$

$$H_e = H + \frac{1}{3}M_L(H). \tag{18}$$

The MMF1 expression for the initial susceptibility coincides with that from the HTA given in Eq. (16).

Second-order modified mean-field model. Ivanov and Kuznetsova performed a rigorous analysis of the pair-correlation functions in dipolar fluids (employing the Yvon-Born-Bogolyubov-Green-Kirkwood formalism [12]) to generate expressions for $M(H)$ and χ [20,21]. What sets this study apart from the others is that the resulting expressions are generated systematically rather than heuristically. The resulting expressions are of a similar form to those of the MMF1 theory, but with modified effective-field terms:

$$M(H) = \rho\left\langle \mu(x)L\left(\frac{\mu_0\mu(x)H_e}{k_BT}\right)\right\rangle, \tag{19}$$

$$H_e = H + \frac{1}{3}M_L(H)\left(1 + \frac{1}{48}\frac{dM_L(H)}{dH}\right). \tag{20}$$

This theory is therefore referred to as the second-order modified mean-field (MMF2) model. The MMF2 expression for the initial susceptibility is (to order χ_L^3)

$$\chi = \chi_L\left(1 + \frac{1}{3}\chi_L + \frac{1}{144}\chi_L^2\right). \tag{21}$$

Cluster expansion theory. Huke and Lücke put forward a cluster-expansion (CE) theory of polydisperse hard spheres [22,23]. This employed a density expansion involving the Mayer f function [12] and the packing fraction $\phi = \pi\rho\langle\sigma^3\rangle/6$ derived from the distribution of the hard-sphere diameter σ, in combination with a perturbation expansion in terms of the dimensionless coupling parameter $\lambda = \mu_0\langle\mu^2\rangle/4\pi k_BT\langle\sigma^3\rangle$. Briefly, the final results are of the form

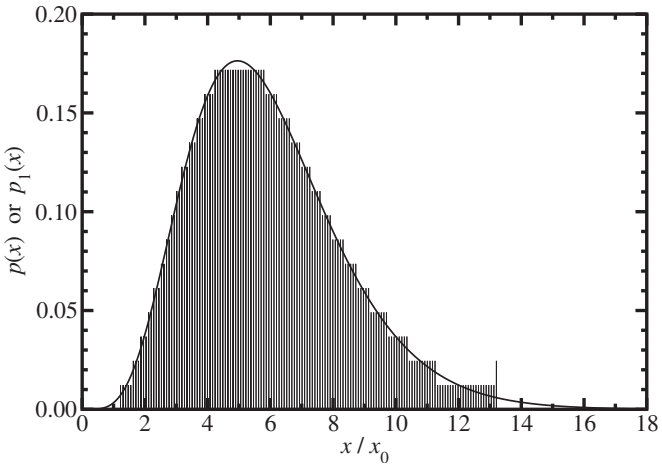

FIG. 1. Magnetic-core diameter distribution functions: $p(x)$ (3) with $a=4.9518$ and $x_0=1.2266$ nm (line); $p_1(x)$ for configuration 1 ($N=1000$ particles) with $1.5 \leqslant x \leqslant 16.4$ nm and $\Delta x=0.1$ nm (impulses).

$$M(H) = \sum_{m=0}^{\infty}\sum_{n=0}^{\infty} G_{mn}\phi^m\lambda^n, \tag{22}$$

where G_{mn} are expansion coefficients that depend on an effective (Weiss) field $H_e = H + \frac{1}{3}M(H)$ and averages of $p(\sigma)$. Note that a low-order expansion of this type has also been presented and tested against simulations by Kristóf and Szalai [26]. The CE initial susceptibility has the same form as the MMF2 expression [see Eq. (21)].

C. Simulation configurations

The aim of performing simulations is to determine the properties of a polydisperse ferrofluid with a prescribed magnetic-core diameter distribution $p(x)$. The determination of $p(x)$ from experimental measurements is described in Sec. III A, but the main result is that $p(x)$ is given by Eq. (3) with the parameters

$$\alpha = 4.9518, \tag{23}$$

$$x_0 = 1.2266 \text{ nm}. \tag{24}$$

In order to carry out simulations with a fixed number of particles, the distribution should be discretized. This can be done in a number of ways, but in this work two different configurations were studied.

In configuration 1, containing $N=1000$ particles, the distribution was discretized with evenly spaced fractions at intervals of $\Delta x=0.1$ nm with the smallest and largest magnetic-core diameters equal to $x=1.5$ nm and $x=16.4$ nm, respectively. The number of particles with diameter x was determined by taking the nearest integer to $Np(x)\Delta x$. To make up the total number of particles to $N=1000$, an extra particle was included with the maximum diameter (above which $Np(x)\Delta x \leqslant \frac{1}{2}$). The resulting discretized distribution, $p_1(x)$, is plotted in Fig. 1 along with the exact curve. The plot suggests that $p_1(x)$ is a faithful repre-

TABLE I. The first six moments $\langle x^n\rangle/x_0^n$ of the discretized simulation distributions $p_1(x)$ and $p_2(x)$, and the exact distribution $p(x)$ defined in Eqs. (3), (23), and (24). Also shown are the percentage deviations between the simulation and exact values.

n	1	2	3	4	5	6
Exact	5.9518	41.376	329.01	2945.2	29310	321003
p_1	5.8684	40.112	309.78	2641.4	24394	240104
% error	−1.4	−3.1	−5.8	−10	−17	−25
p_2	5.9360	41.432	330.75	2964.3	29404	319036
% error	−0.27	+0.14	+0.53	+0.65	+0.32	−0.61

sentation of $p(x)$, but in fact there are some significant differences. In Table I the first six moments of $p_1(x)$ are compared with those of $p(x)$. The percentage deviations increase with increasing n, and at $n=6$ there is a 25% discrepancy. In Sec. III B it will be shown that the deviations lead to a significant disagreement between experiment and simulation.

In configuration 2, containing $N=500$ particles, the magnetic-core diameters were dispersed in a different way. The discretization is based on a fixed number of discrete fractions, each containing N_i particles with diameter $x_i=(i-\frac{1}{2})\Delta x$, the spacing Δx being an adjustable parameter. The number of particles in each fraction is given by the nearest integer to

$$N\int_{x_i-\Delta x/2}^{x_i+\Delta x/2} p(x)dx. \tag{25}$$

The number of fractions (and hence the largest particle diameter) is limited by there being at least one particle in each fraction. With an appropriate choice of Δx, a discretized distribution, $p_2(x)$, can be produced which is faithful to the parent Γ distribution, with moments in close agreement with the exact values. Nine distinct fractions were chosen with $\Delta x=2x_0$, which was found to yield values for the first six moments of $p_2(x)$ within 1% of the exact values. The first six moments are reported in Table I, along with the percentage deviations from the exact values. In Fig. 2 we show $p_2(x)$ along with the exact distribution $p(x)$. Also indicated in the figure are the numbers of particles in each fraction (with magnetic core diameter $x/x_0=1,3,5,\ldots,17$) of the $N=500$ particle configuration.

D. Molecular dynamics

Canonical (NVT) MD simulations were performed with either $N=1000$ or $N=500$ dipolar soft spheres (configurations 1 and 2, respectively) in a cubic simulation cell of side L with periodic boundary conditions applied, and with a Langevin thermostat to effect constant-temperature conditions [24,27–29]. The soft-sphere (Weeks-Chandler-Andersen) potential is

$$u^{SR}(r_{ij})=\begin{cases}4\epsilon\left[(\sigma_{ij}/r)^{12}-(\sigma_{ij}/r)^6+\frac{1}{4}\right] & r<2^{1/6}\sigma_{ij}\\ 0 & r\geq 2^{1/6}\sigma_{ij}\end{cases}, \tag{26}$$

where the range parameter is given by $\sigma_{ij}=(\sigma_i+\sigma_j)/2$, and the energy parameter (ϵ) is assumed equal for all pairs. The

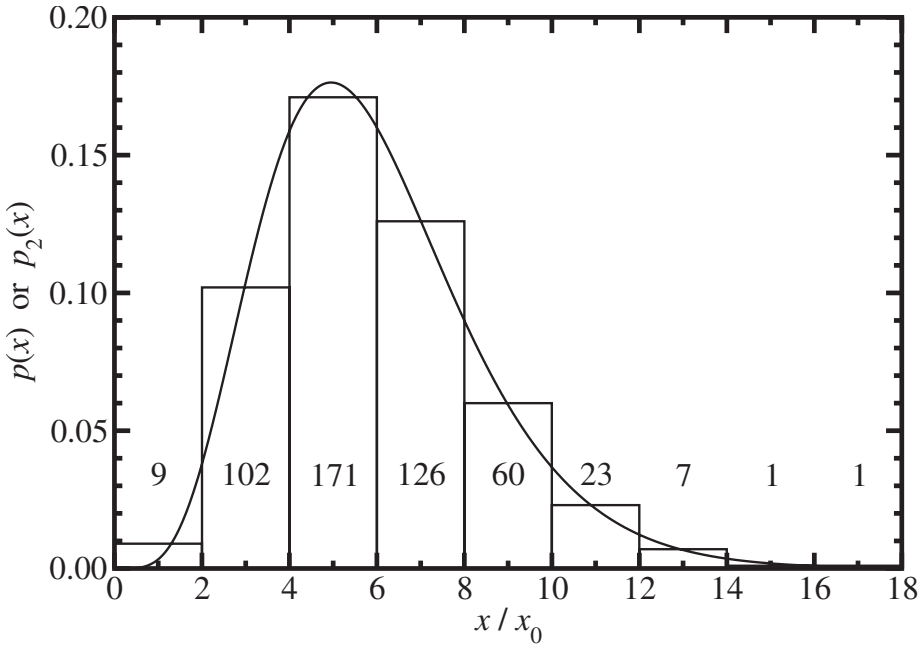

FIG. 2. Magnetic-core diameter distribution functions: $p(x)$ (3) with $a=4.9518$ and $x_0=1.2266$ nm (line); $p_2(x)$ for configuration 2 ($N=500$ particles) with $\Delta x=2x_0$ (bars). Also shown are the numbers of particles in each fraction (with magnetic core diameter $x/x_0=1,3,5,\ldots,17$).

range parameter σ_i for particle i was identified with its magnetic-core diameter x_i. Ignoring hydrodynamic interactions, the Langevin equations of motion for particle i are [30,31]

$$m_i \dot{\mathbf{v}}_i = \boldsymbol{F}_i - \zeta^T \mathbf{v}_i + \boldsymbol{\xi}_i^T, \tag{27}$$

$$\boldsymbol{I}_i \cdot \dot{\boldsymbol{\omega}}_i = \tau_i - \zeta^R \boldsymbol{\omega}_i + \boldsymbol{\xi}_i^R, \tag{28}$$

where m_i is the mass, $\boldsymbol{I}_i$ is the inertia tensor, $\mathbf{v}_i$ ($\boldsymbol{\omega}_i$) is the linear (angular) velocity, $\boldsymbol{F}_i$ ($\boldsymbol{\tau}_i$) is the net conservative force (torque) acting on the particle, ζ^T (ζ^R) is the translation (rotational) friction coefficient, and $\boldsymbol{\xi}_i^T$ ($\boldsymbol{\xi}_i^R$) is the random Brownian force (torque) acting on the particle from an implicit solvent. The vector components of $\boldsymbol{\xi}_i^T$ and $\boldsymbol{\xi}_i^R$ are drawn independently from Gaussian distributions with moments

$$\langle \boldsymbol{\xi}_i^T \rangle = 0, \tag{29}$$

$$\langle \boldsymbol{\xi}_i^T(t) \cdot \boldsymbol{\xi}_j^T(t') \rangle = 6k_B T \zeta_i^T \delta_{ij} \delta(t-t'), \tag{30}$$

$$\langle \boldsymbol{\xi}_i^R \rangle = 0, \tag{31}$$

$$\langle \boldsymbol{\xi}_i^R(t) \cdot \boldsymbol{\xi}_j^R(t') \rangle = 6k_B T \zeta_i^R \delta_{ij} \delta(t-t'). \tag{32}$$

The equations of motion were integrated using the leapfrog algorithm, and the particle orientations were represented using quaternions; the integration scheme was implemented as described in Sec. 3.3.1 of Ref. [24], and in earlier work [28]. It is assumed that each particle's magnetic dipole moment is blocked, i.e., that the dipole moment is static within the particle's body-fixed frame. Therefore, in the simulations, dipole reorientation occurs only by particle rotation (driven by dipolar and Brownian torques), and not by the Néel relaxation (spin flipping) mechanism. For small magnetite particles ($x \lesssim 10$ nm) in kerosene, the time scale for spin flipping is significantly shorter than that for particle rotation [1]. In the present case, the distinction is irrelevant because we are interested only in *static* canonical-ensemble averages, and therefore the dynamical mechanism of establishing equilibrium in the simulations can be selected purely on considerations of computational convenience and efficiency.

MD simulations were carried out in reduced units defined by the mass (m_0) and diameter (d_0) of the smallest particles in the system, and the energy parameter ϵ. All calculations were performed at a temperature $k_B T = \epsilon$, and with a time step $\Delta t = 0.002\sqrt{m_0 d_0^2/\epsilon}$. The friction coefficients were set equal to $\zeta^T = 10.0\sqrt{m_0 \epsilon / d_0^2}$ and $\zeta^R = 3.0\sqrt{m_0 d_0^2 \epsilon}$. The moment of inertia was set equal to $I = 0.4 m_0 d_0^2$ corresponding to a solid sphere of diameter d_0. It was established in Ref. [28] that these simulation parameters lead to reliable results. The long-range dipolar interactions were handled using Ewald sums with conducting boundary conditions. A typical simulation consisted of 5×10^4 time steps for equilibration, followed by a production run of a further 2×10^5 time steps. The magnetization curve $M(H)$ was computed by applying an external magnetic field in the z direction, and computing the ensemble average of the magnetization parallel to the field, i.e., $M = \langle \Sigma_{i=1}^N \mu_{iz} \rangle$ where μ_{iz} is the z component of the dipole moment on particle i.

E. Monte Carlo

Canonical (NVT) MC simulations were performed with $N = 500$ dipolar hard spheres (configuration 2) in a cubic simulation cell of side L with periodic boundary conditions applied [24]. The hard-sphere potential is

$$u^{SR}(r_{ij}) = \begin{cases} \infty & r < \sigma_{ij} \\ 0 & r \geqslant \sigma_{ij} \end{cases}, \tag{33}$$

where $\sigma_{ij} = (\sigma_i + \sigma_j)/2$ is the distance of closest approach of two hard spheres with diameters σ_i and σ_j. The magnetic-core diameters were dispersed according to $p_2(x)$, and the corresponding hard-sphere diameters were given by $\sigma_i = x_i + \sigma_0$, with $\sigma_0 = 2\delta + 2l = 6$ nm. The simulations were conducted using reduced units defined in terms of $\sigma_0 = 6$ nm and the thermal energy $k_B T$ (with $T = 293$ K). Dipolar interactions were handled using the Ewald summation with conducting boundary conditions [24]: the convergence parameter was set equal to $\alpha = 5.6 L^{-1}$, and the reciprocal-space sum was restricted to wave vectors with moduli $|\boldsymbol{k}| \leqslant 6 \times 2\pi/L$. One MC cycle consisted of a trial displacement and a trial rotation for each of N randomly selected particles. Maximum translational and orientational displacements were adjusted to give 20% and 50% acceptance rates, respectively. For each concentration and field strength, the fluid was equilibrated for 5×10^4 cycles, and then simulated in a production run of another 5×10^4 cycles. Longer zero-field simulations (of 10^6 MC cycles after equilibration) were performed to estimate the initial susceptibility using the fluctuation formula appropriate to conducting boundary conditions,

$$\chi = \frac{\mu_0 \langle |\boldsymbol{M}|^2 \rangle}{3 k_B T V}, \tag{34}$$

where $\boldsymbol{M} = \Sigma_{i=1}^N \boldsymbol{\mu}_i$ is the instantaneous magnetic dipole moment of the simulation cell. Long runs were required to ensure that the components of the average magnetization $\langle \boldsymbol{M} \rangle$ were zero within the statistical uncertainties.

III. RESULTS

A. Extracting moments of $p(x)$ from experimental measurements of $M(H)$

Characterizing a ferrofluid suspension boils down to determining the magnetic particle number density ρ, the fluid saturation magnetization M_∞, and the Γ-distribution parameters α and x_0. The "magnetogranulometric" analysis for extracting these parameters has been described many times before [8], and so only the essential elements are described here. In this section are reported results for M_∞ and some moments of $p(x)$ as determined from the theories summarized in Sec. II B. In all cases *except* the MMF2 theory, least-squares fits were made to the complete magnetization curves. This procedure may hide inadequacies of the theories, and may lead to deviations from certain exact asymptotic rela-

tionships. A more obvious side effect of this procedure is a nonmonotonic variation in the fit parameters with increasing concentration, whereas a monotonic drift might be expected of a theory which was steadily applied beyond its limits.

In the case of the MMF2 theory, the third and sixth moments of $p(x)$ were obtained by fitting separately to the weak-field and strong-field portions of the magnetization curves. To obtain consistent values for M_∞, one needs to consider the asymptotic variation of $M(H)$ at very high fields. In this regime, the interparticle interactions are insignificant compared to the particle-field interaction, and hence the one-particle Langevin model becomes asymptotically correct (to order $1/H$):

$$M(H) \approx M_\infty - \frac{\rho k_B T}{\mu_0 H}. \tag{35}$$

The weak-field asymptotics of $M(H)$ yield the Langevin susceptibility, which in turn yields the mean squared magnetic moment $\langle \mu^2 \rangle \propto \langle x^6 \rangle$. Once $\langle x^3 \rangle$ and $\langle x^6 \rangle$ are determined, Eq. (4) can be solved for α and x_0.

The experimental results (taken at $T=293$ K) were presented and analyzed by Pshenichnikov *et al.* in Ref. [8]: ferrofluids at seven different concentrations are referred to by the values of M_∞, these being (in order of increasing concentration) 5.0, 7.8, 11.2, 16.9, 25.3, 37.8, and 57.0 kA m^{-1}. The theories summarized in Sec. II B all give the same leading-order term as Eq. (35), but differ in terms of order $1/H^2$. Nonetheless, it has been noted before that the values of M_∞ are quite insensitive to the specific theory being employed, particularly when experimental measurements at very high fields are available (as is the case here) [8].

A comparison of the Langevin, Weiss, MSA, HTA, and MMF1 models has been presented before [8] in terms of the mean particle diameter $\langle x \rangle$, and the relative width of the distribution. Following Ref. [8], we supplement this comparison with new values of the moments $\langle x^n \rangle$ extracted from the same experimental data using the MMF2 and CE theories. In Table II we show $\langle x^n \rangle$ for the ferrofluid at seven different concentrations but with the *same* magnetic-core diameter distribution (since the different samples were produced by dilution of a concentrated stock sample). The key observation on all of the theories *except* MMF2 is that the apparent mean core diameter $\langle x \rangle$ varies significantly with concentration, by up to 23% with respect to the values at the lowest concentration. There is general agreement between the theories at the lowest concentrations, since in this regime interparticle interactions are quite insignificant. This clearly indicates that at the higher concentrations, interparticle interactions are not being described faithfully by the choices of effective field H_e. Another unsatisfactory property of these results is that there is some degree of scatter, militating against a monotonic variation with concentration; this probably arises from the global, least-squares fitting procedure noted above. It is quite clear that MMF2 yields superior results, with the apparent values of $\langle x \rangle$ remaining essentially constant. Note that these results are obtained through fitting to the weak-field and strong-field regions of the magnetization curves only; it will be shown in Secs. III B and III C that the intermediate portions of the curves are in excellent agreement with experiment.

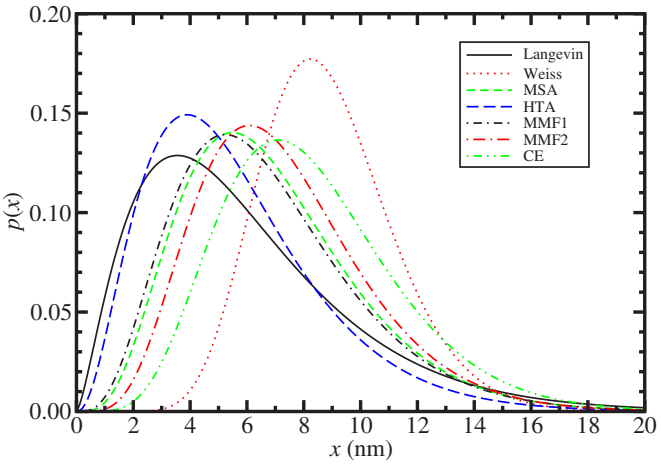

FIG. 3. (Color online) Magnetic-core diameter distributions obtained from the apparent third and sixth moments extracted from experimental data at high concentration ($M_\infty=57.0$ kA m^{-1}) using various theories.

The second, third, and sixth moments evidence similar deviations between the theories. For most of the theories, the variations in the apparent values of $\langle x^n \rangle$ are very significant, but with a general agreement at the lowest concentration. Note the nonmonotonic variations of the parameters with increasing concentration, signaling problems. Significantly, the sole exception is the MMF2 model, which achieves essentially constant values for all of the moments at all concentrations.

The effects of these variations on the derived distributions $p(x)$ are significant. In Fig. 3 a comparison is made between distributions with values of α and x_0 determined from the third and sixth moments reported in Table II for the highest-concentration sample ($M_\infty=57.0$ kA m^{-1}). The variations are large, with the Weiss theory lying far beyond the others. At

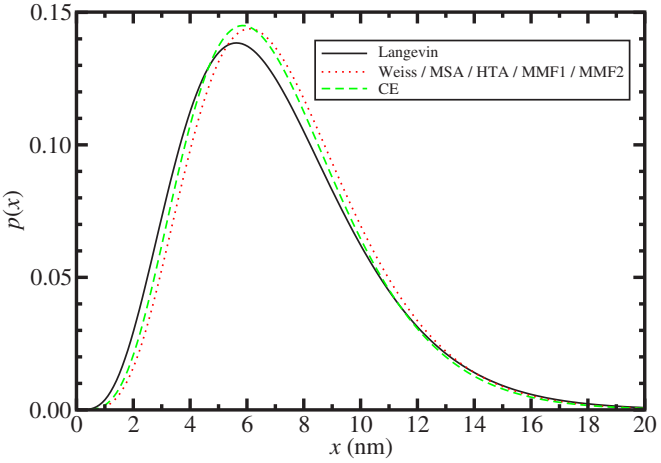

FIG. 4. (Color online) Magnetic-core diameter distributions obtained from the apparent third and sixth moments extracted from experimental data at low concentration ($M_\infty=5.0$ kA m^{-1}) using various theories. The results from Weiss, MSA, HTA, MMF1, and MMF2 theories are identical.

TABLE II. Selected moments of the distribution $p(x)$, $\langle x \rangle$ as extracted from experimental measurements using various theories.

Ref.	Langevin [13]	Weiss [14,15]	MSA [17]	HTA [18,19]	MMF1 [8]	MMF2 [20,21]	CE [22,23]
$M_\infty \downarrow$				$\langle x \rangle$/nm			
5.0	7.1	7.3	7.3	7.3	7.3	7.3	7.1
7.8	7.2	7.6	7.5	7.4	7.5	7.3	7.1
11.2	7.0	7.7	7.5	7.4	7.5	7.3	7.1
16.9	6.4	7.6	7.1	6.9	7.1	7.3	7.2
25.3	6.3	8.0	7.2	6.7	7.1	7.3	7.2
37.8	6.3	8.5	7.2	6.5	7.1	7.3	7.5
57.0	6.0	8.9	6.9	5.6	6.8	7.3	8.2
$M_\infty \downarrow$				$\langle x^2 \rangle / 10$ nm^2			
5.0	6.0	6.2	6.2	6.2	6.2	6.2	6.0
7.8	6.2	6.7	6.6	6.4	6.6	6.3	6.0
11.2	6.0	6.8	6.6	6.4	6.6	6.2	6.0
16.9	5.3	6.7	6.0	5.8	6.1	6.2	6.0
25.3	5.3	7.2	6.2	5.5	6.1	6.2	6.2
37.8	5.4	7.9	6.2	5.2	6.0	6.2	6.5
57.0	5.1	8.4	5.7	4.1	5.6	6.2	7.8
$M_\infty \downarrow$				$\langle x^3 \rangle / 10^2$ nm^3			
5.0	5.9	6.1	6.1	6.1	6.1	6.1	5.7
7.8	6.3	6.7	6.6	6.3	6.6	6.1	5.8
11.2	6.0	6.9	6.6	6.4	6.7	6.1	5.7
16.9	5.4	6.7	5.9	5.7	6.0	6.1	5.9
25.3	5.5	7.3	6.2	5.3	6.0	6.1	6.0
37.8	5.8	8.0	6.2	4.9	5.9	6.1	6.5
57.0	5.5	8.4	5.6	3.7	5.4	6.1	8.3
$M_\infty \downarrow$				$\langle x^6 \rangle / 10^6$ nm^6			
5.0	1.2	1.1	1.1	1.1	1.1	1.1	1.0
7.8	1.4	1.3	1.3	1.2	1.3	1.1	1.0
11.2	1.4	1.3	1.3	1.3	1.4	1.1	1.0
16.9	1.4	1.3	1.2	1.2	1.3	1.1	1.1
25.9	1.6	1.3	1.3	1.0	1.3	1.1	1.1
37.8	2.1	1.3	1.3	0.9	1.2	1.1	1.3
57.0	2.1	1.2	1.1	0.7	1.1	1.1	1.8

low concentrations, the theories should converge since interparticle correlations will then be not so pronounced. The results for the $M_\infty = 5.0$ kA m^{-1} sample are shown in Fig. 4, and clearly demostrate a collapse of the data on to the "correct" distribution. One point should be stressed, however: from Table II, the third and sixth moments from the MMF2 theory are essentially constant over the whole concentration range, and hence α, x_0, and $p(x)$ are also invariant. This is a sign that the MMF2 theory provides a consistent account of interparticle correlations over the whole concentration range considered in this work.

The main conclusion is that of all the theories compared in Table II and Figs. 3 and 4, only the MMF2 theory provides a constant set of moments over a wide range of concentrations. In turn, this means that a reliable determination of $p(x)$ can, at present, only be obtained from the MMF2 theory. Using Eq. (4) and the apparent values of the third and sixth moments extracted using MMF2 theory ($\langle x^3 \rangle \simeq 607$ nm^3 and $\langle x^6 \rangle \simeq 1.09 \times 10^6$ nm^6, respectively) the values of α and x_0 are as given (to four decimal places) in Eqs. (23) and (24). (In consideration of space, the moments presented in Table II were rounded off to two significant figures.) Interparticle correlations become more significant with increasing concentration, but the fact that the apparent distribution obtained using MMF2 theory is essentially invariant with concentration suggests that the theory is providing an accurate account of those correlations through an appropriate specification of H_e. This claim can be tested by a full comparison of $M(H)$ from experiment, MMF2 theory, and computer simulation.

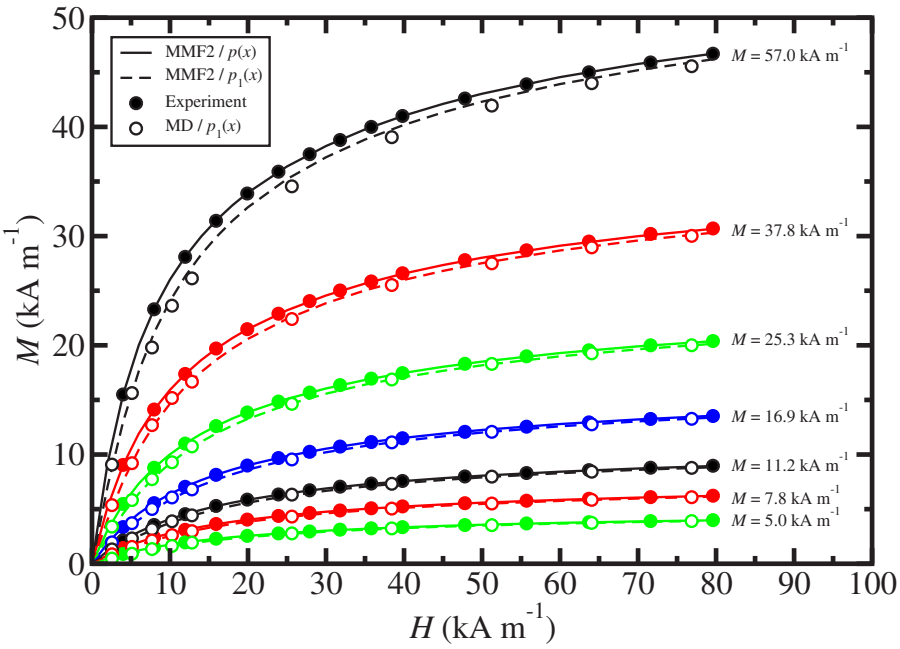

FIG. 5. (Color online) Low-field portions of the magnetization curves, $M(H)$, for ferrofluids at different concentrations with saturation magnetizations (from top to bottom) M_∞=57.0, 37.8, 25.3, 16.9, 11.2, 7.8, and 5.0 kA m^{-1}. Filled circles are from experiment [8], open circles are from MD simulations with $p_1(x)$, solid lines are from MMF2 theory with $p(x)$, and dashed lines are from MMF2 theory with $p_1(x)$.

B. Comparison between experiment, theory, and MD simulations with configuration 1

MD simulations with configuration 1 [$p_1(x)$] were the first to be carried out in this study, but the comparison between the MD and experimental magnetization curves was not very successful. Nonetheless, it is instructive to discuss the origins of the deviations; the results highlight the fact that care must be taken whenever strong polydispersity is being represented in finite-size systems. Magnetization curves at low field ($H \leqslant 80$ kA m^{-1}) from experiment, MMF2 theory, and MD simulations with $p_1(x)$ are shown in Fig. 5. There is essentially perfect agreement between experiment and MMF2 theory with $p(x)$ over the whole range of ferrofluid concentrations considered. This is a necessary but not sufficient condition to claim that MMF2 theory is "correct" because the theory is, in essence, fitted to experiment albeit with only two parameters (α and x_0). To cement this claim the MMF2 theory should match up with simulations of a system with a prescribed composition, such as $p_1(x)$; and if $p_1(x)$ is constructed correctly then experiment, theory, and MD simulation should all agree with each other. Unfortunately, the MD results show significant deviations from experiment and the MMF2 theory with $p(x)$; but this is due to the large deviations in the moments of $p_1(x)$ from the exact values (shown in Table I). To back up this claim, Fig. 5 also shows the predictions of MMF2 theory with $p_1(x)$; recall that the angled brackets in Eq. (19) denote an average over an arbitrary magnetic-core diameter distribution function. The agreement between MD simulations and MMF2 theory with $p_1(x)$ is excellent, and since the MD simulations provide essentially exact results for a given composition, this provides further evidence for the reliability of the MMF2 theory.

C. Comparison between experiment, theory, and MC and MD simulations with configuration 2

Motivated by the discrepancy between experiment and MD simulation data, a more careful discretization of $p(x)$ was carried out, resulting in configuration 2 with $p_2(x)$ as shown in Fig. 2. Table I shows that $p_2(x)$ provides a faithful representation of $p(x)$, at least in terms of the first six moments, despite containing a relatively small number of particles and fractions. Magnetization curves at low field ($H \leqslant 80$ kA m^{-1}) from experiment, MMF2 theory, and MC and MD simulations with $p_2(x)$ are shown in Fig. 6. The predictions of MMF2 theory with $p(x)$ and $p_2(x)$ are almost identical and are not clearly distinguished on the scale of Fig. 6. In part, this is a consequence of an accurate discretization of $p(x)$. The overall agreement between experiment, theory, and simulation is excellent. The coincidence of the MD results for a soft-sphere potential and the MC results for a hard-sphere potential confirms that the precise nature of the short-range potential does not significantly affect the observed magnetic properties [20].

Figure 7 shows the results over the whole range of fields studied in the experimental work, up to $H \simeq 800$ kA m^{-1}. By any measure, the agreement between experiment, MMF2 theory, and MC and MD simulations with $p_2(x)$ is excellent, suggesting that MMF2 theory provides a reliable link between experimental magnetization curves and the parameters of the magnetic-core diameter distribution function. Note that the MMF2 theory was fitted using only the weak-field and strong-field portions of the magnetization curves, and yet the agreement with the experimental results is excellent over the entire range.

Predictions for the initial susceptibility χ from Langevin, Weiss, MSA, HTA/MMF1, and MMF2/CE approaches, and MC simulations are shown as plots of χ against χ_L in Fig. 8. The Langevin susceptibility for the simulated system was computed using Eq. (8) with the appropriate value of $\langle x^6 \rangle$ from $p_2(x)$, and not with the exact value from $p(x)$, although it makes no practical difference. The agreement between the Weiss theory, MSA, HTA/MMF1 theories, MMF2/CE theories, and MC simulations is very good at low concentrations (for which $\chi \lesssim 1$ and $M_\infty \lesssim 16.9$ kA m^{-1}). At higher concen-

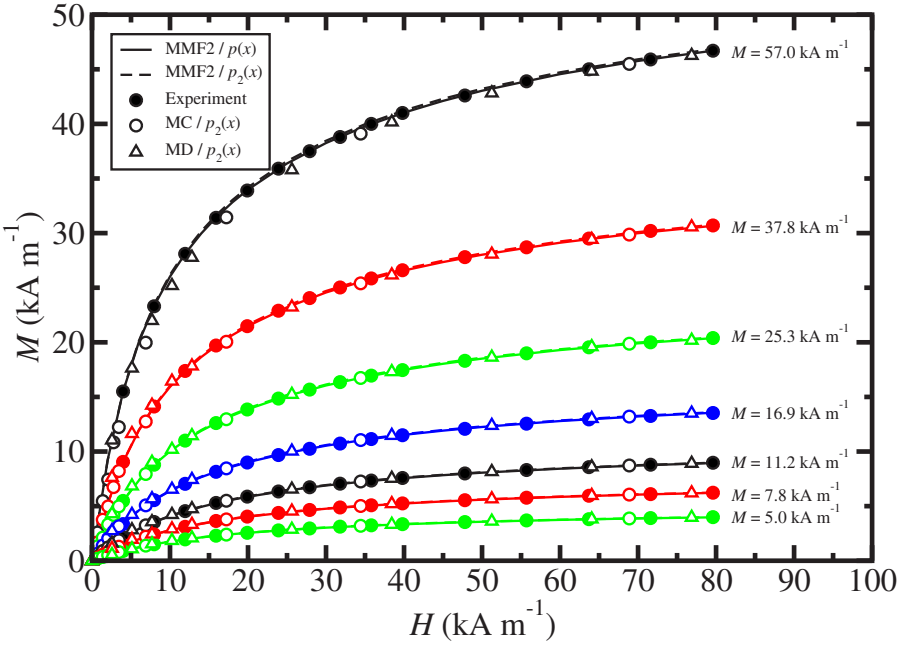

FIG. 6. (Color online) Low-field portions of the magnetization curves, $M(H)$, for ferrofluids at different concentrations with saturation magnetizations (from top to bottom) M_∞=57.0, 37.8, 25.3, 16.9, 11.2, 7.8, and 5.0 kA m^{-1}. Filled circles are from experiment [8], open circles are from MC simulations with $p_2(x)$, open triangles are from MD simulation with $p_2(x)$, solid lines are from MMF2 theory with $p(x)$, and dashed lines (almost coincident with solid lines) are from MMF2 theory with $p_2(x)$. The statistical uncertainties in the simulation points are smaller than the symbol size.

trations the MMF2 curve lies slightly below the simulation results, and the HTA/MMF1 and MSA curves lie lower still. At very high concentrations more significant deviations should be apparent, although this is not easy to demonstrate in the present case because the hard-core packing fraction is considerable at the highest ferrofluid concentration ($\phi \simeq 0.53$), and extending the simulations to higher densities will introduce problems with sampling the polydisperse fluid, and could possibly lead to glassy states. Overall, though, there is a very good correspondence between MMF2/CE theories and MC simulation.

To sum up, MC and MD simulation results should be essentially exact for a system with pairwise additive interactions and a prescribed $p(x)$, in the sense that positional and orientational correlations of all orders can develop between the particles. The observed excellent agreement with experiment is dependent on there being an accurate determination of $p(x)$ (through α and x_0). This implies that the MMF2 theory is providing a consistent and correct account of the long-range dipolar correlations over the full range of ferrofluid concentrations studied in experiment.

IV. CONCLUSIONS

In this paper, experimental measurements of the magnetization curves of polydisperse ferrofluids have been analyzed using a combination of theory and computer simulation. The main objective was to establish a reliable method for the determination of the magnetic-core diameter distribution from experimental measurements. This is achieved by fitting

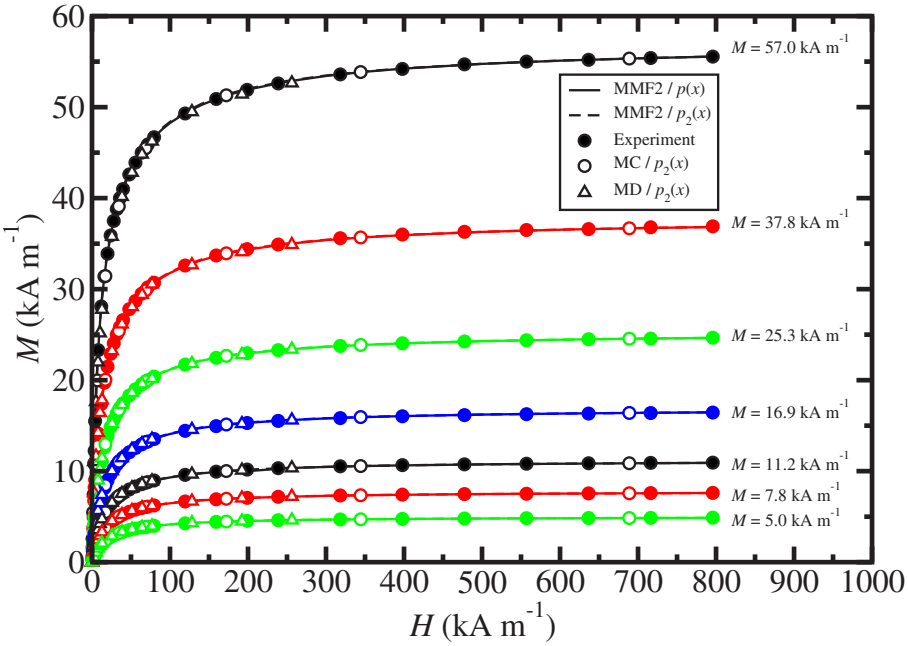

FIG. 7. (Color online) Complete magnetization curves, $M(H)$, for ferrofluids at different concentrations with saturation magnetizations (from top to bottom) M_∞ =57.0, 37.8, 25.3, 16.9 kA m^{-1}, 11.2, 7.8, and 5.0 kA m^{-1}. Filled circles are from experiment [8], open circles are from MC simulations with $p_2(x)$, open triangles are from MD simulation with $p_2(x)$, solid lines are from MMF2 theory with $p(x)$, and dashed lines (almost coincident with solid lines) are from MMF2 theory with $p_2(x)$. The statistical uncertainties in the simulation points are smaller than the symbol size.

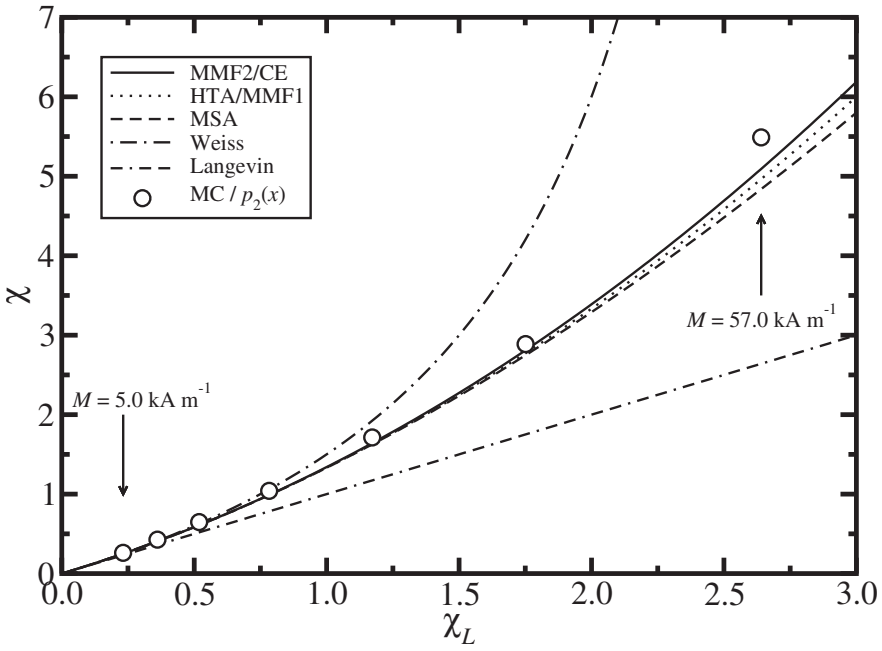

FIG. 8. Initial susceptibility χ vs Langevin susceptibility χ_L from the Langevin theory (dot double-dashed line), Weiss theory (dot-dashed line), MSA (dashed line), HTA/MMF1 theories (dotted line), MMF2/CE theories (solid line), and MC simulations with $p_2(x)$ (open circles). The simulation points correspond to systems with saturation magnetizations of, from left to right, M_∞ =5.0, 7.8, 11.2, 16.9, 25.3, 37.8, and 57.0 kA m^{-1}. The statistical uncertainties in the simulation points are smaller than the symbol size.

theoretical predictions for the magnetization curve (which include averages over the distribution) to the experimental data to extract the parameters of the distribution. One of the key criteria for a reliable method is that the distribution should not vary with the concentration of a ferrofluid with fixed composition; in other words, the theory must be self-consistent and provide an accurate representation of the dipolar correlations over a wide range of concentration. It was shown that of all the theories available at present, only the MMF2 theory of Ivanov and Kuznetsova fulfills this criterion.

To test the reliability of the distribution obtained from this theory, molecular dynamics and Monte Carlo simulations were performed with systems possessing prescribed magnetic-core diameter distributions. In the simulations, the distributions were discretized in to finite numbers of fractions. The agreement between simulation and experiment was seen to be very sensitive to the precise method of discretization. It was demonstrated that the discretized distribution must not only resemble the parent continuous distribution in shape, but also possess very accurate moments. With an appropriate discretized distribution, the agreement between experiment, MMF2 theory, and simulation was excellent. The simulations with inaccurate distributions were also extremely useful, because they compared favorably with the theoretical predictions using those distributions, thus providing more evidence for the reliability of the theory. Finally, a comparison was made between theoretical and simulation predictions for the initial susceptibility. Slight deviations are apparent at the upper end of the experimental concentration range, but overall the reliability of the MMF2 theory (and, here, the CE theory) is very good.

Future work will focus on the ranges of concentration and temperature (or dipole moment) over which the MMF2 theory is applicable. At high enough concentrations, for example, strong short-range correlations must come in to play, and significant deviations between theory and simulation are bound to appear. Another avenue for inquiry will be to compare theoretical and simulation results for the microscopic cluster structure of model ferrofluids [32] and the associated features in the structure factor [33] (which will show strong anisotropies in applied fields [34]). This work is in progress.

ACKNOWLEDGMENTS

The authors are grateful to Professor M. Lücke and Dr. B. Huke for performing the CE theory calculations. The collaborative work between A.O.I., S.S.K., A.F.P., and A.V.L. was supported by INTAS Grant No. 03-51-6064. The collaboration between A.O.I., S.S.K., and C.H. was supported by DFG-RBRF Joint Grant Nos. HO 1108/12-1 and 06-02-04019. The work of A.F.P. and A.V.L. was partly supported by CRDF Grant No. PE-009-0. E.N.R. was supported by IMPRS-PMS grant generously provided by the MPI-P. S.S.K. was partly supported by CRDF Grant No. Y3-P-05-11, President RF Grant No. MK-4836.2006.2, the Dynasty Foundation, and MPI-P. A.C. thanks the School of Chemistry at the University of Edinburgh for financial support, and P.J.C. thanks the Royal Society (UK) for supporting a collaborative visit to Ekaterinburg.

[1] R. E. Rosensweig, *Ferrohydrodynamics* (Dover Publications, Inc., New York, 1998).
[2] V. F. Puntes, K. M. Krishnan, and A. P. Alivisatos, Science **291**, 2115 (2001).
[3] K. Butter, P. H. H. Bomans, P. M. Frederik, G. J. Vroege, and A. P. Philipse, Nat. Mater. **2**, 88 (2003).
[4] K. Butter, P. H. Bomans, P. M. Frederik, G. J. Vroege, and A. P. Philipse, J. Phys.: Condens. Matter **15**, S1451 (2003b).
[5] M. Klokkenburg, R. P. A. Dullens, W. K. Kegel, B. H. Erné, and A. P. Philipse, Phys. Rev. Lett. **96**, 037203 (2006).
[6] T. Tlusty and S. A. Safran, Science **290**, 1328 (2000).
[7] K. I. Morozov, A. F. Pshenichnikov, Y. L. Raikher, and M. I. Shliomis, J. Magn. Magn. Mater. **65**, 269 (1987).
[8] A. F. Pshenichnikov, V. V. Mekhonoshin, and A. V. Lebedev, J. Magn. Magn. Mater. **161**, 94 (1996).
[9] P. I. C. Teixeira, J. M. Tavares, and M. M. Telo da Gama, J. Phys.: Condens. Matter **12**, R411 (2000).
[10] B. Huke and M. Lücke, Rep. Prog. Phys. **67**, 1731 (2004).
[11] C. Holm and J.-J. Weis, Curr. Opin. Colloid Interface Sci. **10**, 133 (2005).
[12] J.-P. Hansen and I. R. McDonald, *Theory of Simple Liquids* (Academic Press, London, 1986).
[13] P. Langevin, J. Phys. Theor. Appl. **4**, 678 (1905).
[14] P. Weiss, J. Phys. Theor. Appl. **VI**, 661 (1907).
[15] A. Tsebers, Magnetohydrodynamics **18**, 137 (1982).
[16] M. S. Wertheim, J. Chem. Phys. **55**, 4291 (1971).
[17] K. I. Morozov and A. V. Lebedev, J. Magn. Magn. Mater. **85**, 51 (1990).
[18] Y. A. Buyevich and A. O. Ivanov, Physica A **190**, 276 (1992).
[19] A. O. Ivanov, Magnetohydrodynamics **28**, 353 (1992).
[20] A. O. Ivanov and O. B. Kuznetsova, Phys. Rev. E **64**, 041405 (2001).
[21] A. O. Ivanov and O. B. Kuznetsova, Colloid J. **68**, 430 (2006).
[22] B. Huke and M. Lücke, Phys. Rev. E **62**, 6875 (2000).
[23] B. Huke and M. Lücke, Phys. Rev. E **67**, 051403 (2003).
[24] M. P. Allen and D. J. Tildesley, *Computer Simulation of Liquids* (Clarendon Press, Oxford, 1987).
[25] M. Abramowitz and I. A. Stegun, *Handbook of Mathematical Functions* (Dover Publications, Inc., New York, 1965).
[26] T. Kristóf and I. Szalai, Phys. Rev. E **68**, 041109 (2003).
[27] W. F. van Gunsteren and H. J. C. Berendsen, Mol. Phys. **45**, 637 (1982).
[28] Z. Wang, C. Holm, and H. W. Müller, Phys. Rev. E **66**, 021405 (2002).
[29] Z. W. Wang and C. Holm, Phys. Rev. E **68**, 041401 (2003).
[30] P. G. Wolynes and J. M. Deutch, J. Chem. Phys. **67**, 733 (1977).
[31] E. Dickinson, S. A. Allison, and J. A. McCammon, J. Chem. Soc., Faraday Trans. 2 **81**, 591 (1985).
[32] A. O. Ivanov and S. S. Kantorovich, Phys. Rev. E **70**, 021401 (2004).
[33] P. J. Camp and G. N. Patey, Phys. Rev. E **62**, 5403 (2000).
[34] J. P. Huang, Z. W. Wang, and C. Holm, Phys. Rev. E **71**, 061203 (2005).